[CANCER RESEARCH 52, 4157–4167, August 1, 1992]

Effect of Bivalent Interaction upon Apparent Antibody Affinity: Experimental Confirmation of Theory Using Fluorescence Photobleaching and Implications for Antibody Binding Assays[1]

Eric Neil Kaufman and Rakesh K. Jain[2]

Department of Chemical Engineering, Carnegie Mellon University, Pittsburgh, Pennsylvania 15213-3890 [E. N. K.], and Edwin L. Steele Laboratory, Department of Radiation Oncology, Massachusetts General Hospital, Harvard Medical School, Boston, Massachusetts 02114 [R. K. J.]

ABSTRACT

The affinity of a monoclonal antibody for its tumor-associated antigen is one of several parameters governing *in vivo* monoclonal antibody distribution. However, there is a lack of apparent correlation between the affinity of a bivalent monoclonal antibody measured using equilibrium binding experiments and its *in vivo* delivery. Furthermore, differences in the reported affinity for identical antibody/antigen pairs are quite common in the literature. In this paper, both of these discrepancies are addressed in terms of variation in avidity due to bivalent interaction. The enhancement of avidity afforded by bivalent attachment is addressed theoretically by extending the model of Crothers and Metzger (Immunochemistry, *9:* 341–357, 1972). Theoretical assessment of Lineweaver-Burk, Scatchard, Steward-Petty, Langmuir, fluorescence recovery after photobleaching, and Sips models demonstrates quantitatively that the measured affinity using equilibrium binding experiments may vary over four orders of magnitude with similar variation in experimental cellular antigen density. Further, the measured affinity is a function of the experimental protocol. Predictions of avidity enhancement were confirmed experimentally using fluorescence recovery after photobleaching. These experiments measured the equilibrium binding constant and concentration of binding sites for an immunoglobulin G monoclonal antibody and its F(ab) fragment directed against the rabbit VX2 carcinoma cell line. Bivalent binding data agree quantitatively with those predicted by the bivalent model with no adjustable parameters. It is concluded that bivalent equilibrium binding constants are useful only in antibody screening, where experimental conditions are identical for all series. They must be used with caution in predicting *in vivo* antibody distribution, and it is recommended that the intrinsic, monovalent affinity be measured in tandem with any bivalent antibody study as a standard reference.

INTRODUCTION

The ability to produce monoclonal antibodies reactive with tumor-associated antigen offers the promise of achieving preferential localization of therapeutic agent in tumor as opposed to normal tissue. However, monoclonal antibodies produced to date have not realized this promise, presumably because of their poor localization in large tumors (1). It has been recognized that among the many parameters governing the distribution of antibody to tumor tissue are the equilibrium binding constant of the antibody/antigen interaction, the concentration of antigenic determinants present in the tissue, and the fraction of injected antibody lacking immunoreactivity (examples include Refs. 2–10). Current techniques for the quantification of these parameters designed for either *in vivo* (Footnote 3; Refs. 11 and 12) or *in vitro* (13) experimentation utilize equilibrium solid-phase binding assays. Experimental data are analyzed using a variety of algebraic transformations, all modeling the association reaction as a single-step process with homogeneity in antibody valence. However, in the manner that these assays are conducted, critical parameters for determining antibody valence are varied. This leads to measured parameters which are functions of their experimental conditions rather than intrinsic physical phenomena (13).

Cases are found in the literature where antibody distribution *in vivo* is inconsistent with its measured affinity for the antigen *in vitro* (8, 14, 15). There are also instances in which the reported affinity for identical antibody/antigen pairs varies among laboratories (12, 16–19). The former may be due to differences between *in vivo* and *in vitro* antigen expression (8, 14, 20, 21) or possible problems applying compartmental models in the interpretation of *in vivo* tissue uptake studies. Both inconsistencies may also be explained by varying antibody valence and, hence, varying antibody avidity under different experimental conditions. The IgG[4] antibody is bivalent, capable of binding two antigenic sites under favorable conditions. Obviously bivalent attachment to a tumor cell surface leads to a larger avidity for the surface than monovalent attachment. The augmentation in affinity due to increased valence is often termed an "enhancement factor." Some authors (13) prefer to use the term "affinity" only to describe monovalent interaction and "avidity" when the strength of the interaction is augmented by increased valence. The theoretical formulations of enhancement factors have been derived for many experimental protocols (22–29). Their effects have also been demonstrated in comparisons of measured affinities and dissociation rates for F(ab)

Received 3/11/92; accepted 5/14/92.

The costs of publication of this article were defrayed in part by the payment of page charges. This article must therefore be hereby marked *advertisement* in accordance with 18 U.S.C. Section 1734 solely to indicate this fact.

[1] This work was supported by National Science Foundation Grant CBT-88-16062 and National Cancer Institute Grants CA36902 and CA49792.

[2] To whom requests for reprints should be addressed.

[3] E. N. Kaufman and R. K. Jain. *In vitro* measurement and screening of monoclonal antibody affinity using fluorescence photobleaching, J. Immunol. Methods, in press.

[4] The abbreviations and notations used are: IgG, immunoglobulin G; D, diffusion coefficient (cm^2/s); FRAP, fluorescence recovery after photobleaching; I_{Avg}, average fluorescence intensity in a square area centered about the bleach (gray levels, GL); I_{TB}, fluorescence intensity at the center of the bleach at time equal to zero (GL); I_{TU}, fluorescence intensity far from the bleached region (GL); K, equilibrium association constant assuming single-step, homogeneous binding (M^{-1}); K_1, monovalent equilibrium association binding constant (M^{-1}); K_2, bivalent equilibrium association binding constant (cm^2/mol); erf, error function; f-RVC, fluorescein-labeled RVC antibody; k_1, association binding constant between antibody and antigenic reactive sites ($M^{-1}s^{-1}$); k_{-1}, dissociation constant between antibody- and antigen-reactive sites (s^{-1}); k_2, rate of conversion from monovalent to bivalently bound antibody ($cm^2mol^{-1}s^{-1}$); k_{-2}, dissociation constant between bivalently and monovalently bound antibody (s^{-1}); nr, fraction of incubating antibody lacking biological activity; r_c, cell or bead radius (cm); $_s$, subscript to denote surface concentration; R_o, Gaussian radius of the photobleach (cm); t, time (s); u, dimensionless size of acquisition region; [Ab], concentration of unbound (free) antibody which is biologically active (M); [Ab_T], concentration of incubating antibody (M); [Ab_{inc}], incubating concentration of biologically active antibody (M); [AbAg], concentration of monovalently bound antibody (M); [$AbAg_2$], concentration of bivalently bound antibody (M); [B], total concentration of bound antibody (M); [Ag_o], total concentration of binding sites (M); [Ag], concentration of vacant antigenic binding sites (M); [$Ag]_a$, concentration of vacant binding sites within arm's reach of the monovalently bound antibody (M); $\langle r \rangle$, average distance between antibody binding sites (cm); ϕ_c, fraction of biologically active antibody which is bound; ϕ_o, uncorrected immobile fraction; γ, ratio of microtiter well area to incubating antibody volume (cm^{-1}); E, exponent base 10.

and IgG of identical origin (30–34). The ability of an IgG molecule to bind bivalently is a complex function of the concentration of antibody in solution, the cellular antigen density, and steric constraints of both the antibody and antigen (22). Although IgG antibodies exist in a mixture of monovalently and bivalently bound states on the cell surface, analyses of solid-phase binding assays consider the binding interaction homogeneous in valence. These methods of analysis require measurement of immobilized antibody, as factors affecting antibody valence and, hence, avidity are varied. Deviations from homogeneous valence are theoretically evidenced by deviations from the ideal linear Lineweaver-Burk, Scatchard, and Steward-Petty formulations (27, 35–37). However, both the quality and quantity of experimental data often obscure these anomalies and lead to measured parameters being functions of their experimental conditions.

In this paper, we demonstrate, both theoretically and experimentally, how the presence of bivalent binding causes measured affinities to be reflections more of the experimental protocol than of the physical process they represent. This may explain the lack of apparent correlation between antibody avidity and its *in vivo* distribution in recent studies, as well as the differences in reported affinities for identical antibody/antigen systems. Currently accepted solid-phase assay binding plots for various experimental conditions and protocols are simulated by theoretically generating data using the bivalent binding model of Crothers and Metzger (22) and using regression analysis to obtain the predicted kinetic parameters. The ability of the Lineweaver-Burk plot to correctly predict the fraction of nonreactive antibody is unaffected by varying antibody valence. However, the affinity binding constant obtained through Scatchard analysis may vary over four orders of magnitude, depending upon the surface density of antigen. Even at constant antigen densities, the selection of incubating antibody concentrations as well as the form of immobilized antigen is shown to further affect the resulting kinetic parameters. The equilibrium binding constants and concentration of binding sites for an IgG monoclonal antibody and its F(ab) fragment directed against the rabbit VX2 carcinoma cell line were determined using FRAP. These experimental results confirm the theoretical predictions both qualitatively and quantitatively. In light of the fact that bivalent antibody avidity is not an intrinsic physical parameter, it is recommended that the intrinsic affinity of the monovalent interaction be reported as a standard reference in any antibody binding study.

MATERIALS AND METHODS

Theoretical Assessment of Avidity Enhancement

Analysis of Equilibrium Binding Data. Commonly used forms of solid-phase data analysis model the antibody/antigen interaction as an equilibrium, single-step process, exhibiting homogeneity in binding valence. That is,

$$K = \frac{[B]}{((1 - nr)[Ab_T] - [B])([Ag_o] - [B])} \quad (A)$$

where terms are as defined in Footnote 4.

Various transformations of Equation A lead to the commonly used forms of antibody binding analysis. The Lineweaver-Burk method (38) is used to obtain the fraction of incubating antibody that is biologically unreactive. It requires the experiment to be conducted in great antigen excess (39) so that $[Ag_o - B] \sim [Ag_o]$ and the definition of the equilibrium binding constant may be rearranged to yield

$$\frac{[Ab_T]}{[B]} = \frac{1}{(1 - nr)} + \frac{1}{(1 - nr)K[Ag_o]} \quad (B)$$

Thus, by measuring the ratio of incubating to bound antibody concentrations as the total concentration of binding sites is varied, the Lineweaver-Burk assay yields the nonreactive fraction of incubating antibody from the inverse of the *y* intercept in Equation B. This assay is not utilized for the quantification of the equilibrium binding constant, however, due to the limitations associated with assuming antigen excess.

Once the nonreactive fraction is obtained via Lineweaver-Burk analysis, the equilibrium binding constant and total concentration of binding sites can be obtained by incubating a fixed concentration of antigen (or cells) with varying antibody concentrations. The concentration of antibody both bound to the immobilized antigen and free in solution is measured for each dilution of antibody. A number of graphical methods can be used to extract kinetic parameters from these data (13). The most widely used of these methods are the Scatchard plot (40)

$$\frac{[B]}{[Ab]} = K[Ag_o] - K[B] \quad (C)$$

and the reciprocal or Steward-Petty plot (41)

$$\frac{1}{[B]} = \frac{1}{K[Ag_o][Ab]} + \frac{1}{[Ag_o]} \quad (D)$$

When the experimental data are plotted in the form of Equation C or D, the slope and *y* intercept of the best-fit line through the data yield the total concentration of binding sites and equilibrium binding constant. Another form of analysis is the Langmuir plot (42)

$$[B] = \frac{K[Ag_o][Ab]}{1 + K[Ab]} \quad (E)$$

in which the concentration of bound antibody asymptotically approaches a value of $[Ag_o]$ for large [Ab]. The initial slope of the curve yields the value of *K*. Yet another transformation of Equation A was proposed by Kaufman and Jain (12) for FRAP experiments. These experiments measure the fraction of biologically active antibody which is bound, as a function of antibody and antigen concentrations. This transformation yields

$$\phi_c = \frac{[B]}{Ab_{inc}} = \frac{\frac{1 + K(Ag_o + Ab_{inc})}{KAb_{inc}} - \left[\left(\frac{1 + K(Ag_o + Ab_{inc})}{KAb_{inc}}\right)^2 - \frac{4Ag_o}{Ab_{inc}}\right]^{0.5}}{2} \quad (F)$$

Sips or Hill plots (43, 44) are used as a measure of deviation from the "ideal" of Equation A. The Sips formulation for monovalent binding is

$$\log\left(\frac{r}{1 - r}\right) = a(\log[Ab] + \log(K)) \quad (G)$$

where *r* is equal to $[B]/[Ag_o]$ and *a* is a measure of system nonideality ($a = 1$ being ideal). The value of $[Ag_o]$ used in this analysis may be obtained by any of the above graphical analyses. The Sips equation for purely bivalent binding is

$$\log\left(\frac{r}{2 - r}\right) = a(\log[Ab] + \log(K)) \quad (H)$$

Previous studies have addressed deviations from the "ideal" of Equation A due to heterogeneous antibody and antigen populations (45–51), endocytosis (52), cell clustering (24), diffusion limited binding (53–55),

as well as other factors (13, 35). Studies have also indicated qualitatively that these complicating factors will cause the affinity values obtained to depend upon the region of the binding curve used for calculation (13). Here, we quantitatively demonstrate the magnitude of this dependence due to bivalent interaction by simulating data using a suitable model of bivalent binding and fitting these data to the above-mentioned forms of analysis. We also confirm these predictions experimentally.

Model. The proposed model of bivalent binding is an extension of that derived by Crothers and Metzger (22), using spatial and angular distribution factors, and later reformulated by Perelson *et al.* (26). Our derivation of this model closely follows that of Perelson *et al.* (26). A schematic of this binding interaction is shown in Fig. 1. Biologically active antibody in the bulk solution (Ab) combines reversibly with a vacant antigenic site on the surface (Ag_s) to form a monovalently bound antibody/antigen complex ($AbAg)_s$. If there exist vacant antigen sites in the neighborhood of the monovalently bound antibody, the second binding site on the antibody may reversibly bind to a second antigenic site to form a bivalently bound complex ($AbAg_2)_s$. The antigen is assumed to consist of monovalent hapten to avoid the kinetic complications of antibody crosslinking. The process of monovalent adsorption is characterized by the equilibrium constant

$$K_1 = \frac{k_1}{k_{-1}} = \frac{[AbAg]_s}{2[Ab][Ag]_s}\,[\equiv]\ M^{-1} \qquad (I)$$

and the conversion of monovalent to bivalent antibody adsorption by

$$K_2 = \frac{k_2}{k_{-2}} = \frac{2[AbAg_2]_s}{[AbAg]_s[Ag]_s}\,[\equiv]\ \frac{cm^2}{mol} \qquad (J)$$

The statistical factors of two are introduced due to the fact that, in the first step, IgG can bind at either of its arms but dissociate from only one while in the second the converse is true (13, 27). Subscript "s" denotes surface concentration, and a lack of subscript denotes bulk concentration. As a first-order approximation, the rate at which one arm of the IgG dissociates from an antigenic site is taken to be independent of the valence of binding (23, 26, 56). That is, $k_{-1} = k_{-2}$. While this may not be strictly true due to thermodynamic considerations, lack of detailed knowledge precludes thermodynamic second-order correction. The rate at which monovalently bound IgG becomes bivalently bound will equal the association constant for interactions between antibody sites and vacant antigenic determinants (k_1) multiplied by both the concentration of singly bound IgG ($[AbAg]_s$) and the concentration of vacant antigenic sites within reach of the monovalently bound IgG ($[Ag]_{sa}$) (26). As derived (22, 26), this accessible concentration ($[Ag]_{sa}$) is equal to the mol of antigenic sites found in the area swept out by the average distance between antibody combining sites ($\langle r\rangle$), divided by the volume above the surface swept out by this same radius (Fig. 2; Footnote 5). That is

$$[Ag]_{sa} = \frac{[Ag]_s\pi\langle r\rangle^2}{\frac{2}{3}\pi\langle r\rangle^3} = \frac{3[Ag]_s}{2\langle r\rangle} \qquad (K)$$

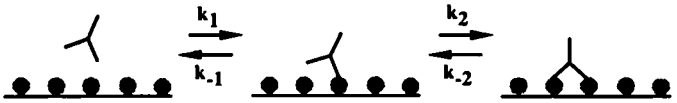

Fig. 1. Schematic of bivalent antibody binding. The bivalent monoclonal antibody in solution at bulk concentration [Ab] reversibly binds to a vacant binding site at surface concentration $[Ag]_s$ to form a monovalently bound complex. The monovalently bound antibody at surface concentration $[AbAg]_s$ may then reversibly combine with a vacant antigenic site within arm's reach of the antibody $[Ag]_s$ to form a bivalently bound complex at surface concentration $[AbAg_2]_s$.

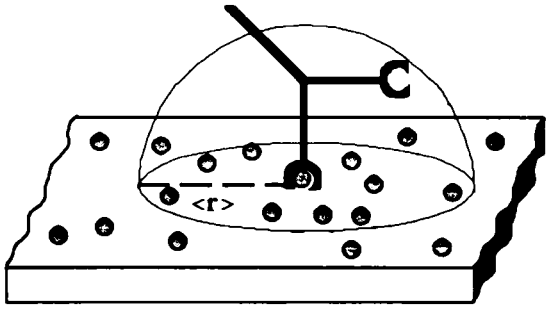

Fig. 2. Accessible binding site concentration. The concentration of vacant binding sites accessible to the monovalently bound antibody is equal to the product of the vacant site surface density and area swept out by the distance between binding sites on the antibody molecule, divided by the volume encompassed by the combining sites.

Thus, the rate of bivalent association is equal to

$$k_2[AbAg]_s[Ag]_s = k_1[AbAg]_s\left(\frac{3[Ag]_s}{2\langle r\rangle}\right) \qquad (L)$$

and the rate constant for monovalent to bivalent conversion

$$k_2 = \frac{3k_1}{2\langle r\rangle} \qquad (M)$$

Dividing Equation M by $k_{-2} = k_{-1}$ leads to the relationship between the two equilibrium binding constants derived by Crothers and Metzger (22).

$$K_2 = \left(\frac{3}{2\langle r\rangle}\right)K_1 \qquad (N)$$

Extending the derivation in Ref. 22, when binding experiments are performed by incubating antibody with cells expressing antigenic sites on their surface, it is convenient to work with bulk rather than surface concentrations. The surface concentration of any component is equal to its bulk concentration divided by the cell surface area per unit volume in the incubating solution. For the case of spherical cells of radius r_c in solution,

$$X_s = \frac{X}{(4\pi r_c^2)\left(\frac{\text{no. of cells}}{cm^3}\right)} \qquad (O)$$

When a total concentration of antigen-specific IgG $[Ab_T]$ with a nonreactive fraction (nr) is incubated with cells which express antigen, the bulk concentration of total antigenic sites ($[Ag_o]$) is equal to

$$[Ag_o] = \frac{\left(\frac{\text{no. of sites}}{\text{cell}}\right)\left(\frac{\text{no. of cells}}{cm^3}\right)\left(\frac{1000\ cm^3}{1}\right)}{\left(\frac{6.022\times10^{23}\ \text{sites}}{\text{mol}}\right)}\,[\equiv]\ M \qquad (P)$$

With this basis, the concentrations of Ab, AbAg, $AbAg_2$, and Ag may be derived for any experimental condition. Mass balances for the total

[5] Crothers and Metzger (22) discuss the implications of using average binding site concentrations rather than a statistical mechanical model of the surface. Their model assumes a random distribution of antigenic sites on the cell surface, with no defined maximum on the local density. Mathematically, this is equivalent to completely mobile antigen. In order for the average concentration of sites to be used in Equation K, the number of vacant sites in an area of $\langle r\rangle^2$ should be much greater than unity. When this assumption is not valid, the bivalent binding model will overestimate the amount of antibody bound bivalently, thus overestimating the observed equilibrium binding constant. In the simulations conducted in this paper with antigen density less than 1×10^5 sites/cell $[Ag]_s\pi\langle r\rangle^2$ is near unity, and bivalent interaction is overestimated. This underestimates both the dependence of the measured equilibrium binding constant upon antigen density and the possible resolution of the binding curve into separate components for systems with low antigen density.

concentration of antibody and antigen and the definitions of the two equilibrium constants (Equations I and J) provide four equations for the four unknown concentrations.

$$[Ab_T] = [Ab] + [AbAg] + [AbAg_2] + nr[Ab_T] \quad (Q)$$

$$[Ag_o] = [Ag] + [AbAg] + 2[AbAg_2] \quad (R)$$

Upon algebraic rearrangement, the following expressions are reached. They enable theoretical simulations of Lineweaver-Burk, Scatchard, Steward-Petty, Langmuir, FRAP, and Sips analyses.

$$[Ag]^3 + [Ag]^2\left(\frac{2}{K_1\Psi} - [Ag_o] + 2[Ab_T](1 - nr)\right) + [Ag]\left(\frac{1}{K_1^2\Psi} + \frac{2([Ab_T](1 - nr) - [Ag_o])}{K_1\Psi}\right) - \frac{[Ag_o]}{K_1^2\Psi} = 0 \quad (S)$$

$$[Ab] = \frac{[Ab_T](1 - nr)}{1 + 2K_1[Ag] + K_1^2\Psi[Ag]^2} \quad (T)$$

$$[AbAg] = 2K_1[Ab][Ag] \quad (U)$$

$$[AbAg_2] = K_1^2\Psi[Ab][Ag]^2 \quad (V)$$

where

$$\Psi = \frac{3}{8\pi r_c^2\langle r\rangle\left(\frac{\text{no. of cells}}{\text{cm}^3}\right)} \quad (W)$$

Equations of similar algebraic form were derived by Reynolds (25) and Dower *et al.* (27) for models in which K_1 and K_2 were unrelated and antigen was fully mobile on the cell surface. The observed equilibrium binding constant (assuming the model of Equation A) for a given set of experimental conditions is given by

$$K_{obs} = \frac{[AbAg_2]_s + [AbAg]_s}{[Ab][Ag]_s} = K_1(2 + K_2[Ag]_s) \quad (X)$$

Due to our convention of using the concentration of antibody rather than the concentration of antibody binding sites in Equation I, K_{obs} will equal $2K_1$ rather than the monovalent parameter K_1 when IgG is unable to bind bivalently.

Parameters and Methods Used in Simulations. Parameter values used for the monovalent equilibrium constant, cell radius, average distance between binding sites on the antibody molecule, and fraction of incubating antibody lacking biological activity are shown in Table 1. The value of K_1 is based upon that of a moderately binding F(ab) fragment and is slightly less than that for F(ab) fragments screened for clinical use (33). The value of $\langle r\rangle$ is based upon the derivation of Crothers and Metzger (22). It assumes a completely flexible hinge region connecting the two F(ab) fragments and a distance from the hinge region to the end of the F(ab) fragment of 65 Å. To assess the effect of cellular antigen density, the number of antigenic sites per cell was varied between 5×10^3 and 5×10^6 sites per cell. For comparison, antigen densities ranging between 1×10^4 and 1×10^6 sites/cell have been reported in monoclonal antibody/tumor-associated antigen cell binding assays (33, 34, 39, 57, 58).

In Lineweaver-Burk simulations, an initial cellular concentration of 1×10^5 cells/ml was increased by a factor of two for ten successive data points (39, 59). The concentration of incubating antibody was chosen to be a 200-fold dilution of the antibody concentration that would saturate a solution of 2×10^6 cells/ml as per Ref. 59. This ensured antigen excess. The effect of antigenic site density and, hence, magnitude of bivalent interaction on the measured fraction of nonreactive antibody was assessed by fitting this data to Equation B.

Table 1 *Baseline parameters utilized in simulations*

Parameter	Abbreviation	Value
Monovalent equilibrium binding constant	K_1	1×10^7 M^{-1}
Cell radius	r_c	7.5×10^{-4} cm
Av. distance between antibody binding sites	$\langle r\rangle$	8.7×10^{-7} cm
Nonreactive fraction of incubating antibody	nr	0.3
Ratio of microtiter well area to incubating antibody volume	γ	14.14

In simulations to extract the equilibrium binding constant and binding site concentration, the concentration of cells was chosen to be 1×10^6 cells/cm^3 (39). Baseline simulations were conducted using an incubating antibody concentration beginning at 1×10^{-11} M and increasing uniformly over three orders of magnitude. Simulations were performed with varying cellular antigenic site densities to assess the effect of increasing bivalent interaction upon the measured parameters. To investigate how the choice of incubating antibody concentrations influenced measured parameters, simulations were also conducted using initial incubating antibody concentrations between 1×10^{-10} and 1×10^{-12} M. This is within the concentration range used experimentally (39). For these simulations, Equations S to V were used to generate 10 values of bound and free antibody concentrations. These data were then fit to the appropriate equation in order to obtain values for the "measured" bulk concentration of antigenic sites (Ag_o) and equilibrium binding constant (K). In the case of Sips analysis the measured deviation from ideality a was obtained. To eschew many of the complications associated with cell assays, some investigators utilize purified antigen immobilized at high concentrations to cell culture plates as the antigen component in binding assays. These experiments, after a conversion between surface and bulk antigen concentrations (see below), were analyzed with the same methods described above.

Experimental Verification of Avidity Enhancement Model Using FRAP

Theoretical predictions of enhanced avidity were both qualitatively and quantitatively confirmed experimentally using FRAP (Footnote 3; Refs. 11 and 12). The immobile fractions measured for the IgG antibody were predicted by the model of bivalent interaction with no adjustable parameters needed. While this model is an approximation, it is seen that it can be a useful tool in aiding the interpretation of bivalent equilibrium binding experiments when accompanied by monovalent studies.

The use of FRAP to obtain mass transport and binding parameters was developed in our earlier work (Footnote 3; Refs. 11 and 12). The reader is referred to these papers for the mathematical and experimental development of the technique and analysis of model assumptions. In the photobleaching technique, fluorescently labeled antibody is incubated with an immobilized antigen component and is observed using a fluorescence microscope. A laser is used to irreversibly quench the fluorescence in a given region of the specimen. Following the bleaching process, fluorescence intensity recovers in this region due to the diffusion of the fluorescently active, mobile macromolecule into the bleached area. For a reaction-limited binding system (12), the fluorescence intensity *versus* time after photobleaching is defined by the diffusion coefficient of the fluorescent protein and the fraction of

fluorescent protein which is bound to the immobile antigen.[6] By measuring this immobile fraction as the concentration of antibody or antigen is varied, the equilibrium binding constant and concentration of binding sites may be obtained through regression of the data to Equation F.

Samples. IgG (M_r ~150,000) monoclonal antibody RVC-626, directed against the rabbit VX2 carcinoma tumor line (60), and the F(ab) fragment of this antibody (M_r ~50,000) were the kind gifts of D. Mackensen (Hybritech, Inc., San Diego, CA). The antibodies were labeled with fluorescein (Lot C-4685 IgG, Lot C-4706 F(ab); Molecular Probes, Eugene, OR) to yield a dye:protein ratio of 7.5 and 3.4 [IgG and F(ab), respectively] and an antibody concentration of 4.0 and 0.19 mg/ml [IgG and F(ab)]. Sodium Azide (2 mM) was added to the stock antibody to inhibit bacterial growth. In addition, bovine serum albumin (1%) was added to the F(ab) stock, following the labeling procedure, to aid protein stability. Antibody was stored at −72°C. Once thawed or incubated with antigen beads, samples were stored at 5°C. The percentage of fluorescent material lacking antibody reactivity was assessed for both samples using the fluorometric procedure described in Ref. 12. In the equilibrium binding experiments, tumor homogenate containing tumor-associated or irrelevant antigen immobilized to 1.6-μm diameter beads (Lots C061991RB1 and A051491C1, respectively) donated by B. Rhodes (RhoMed, Inc., Albuquerque, NM) was utilized as the immobilized antigen component. The beads were supplied as a 2% by volume solution of beads in PBS and 1% bovine serum albumin. In binding experiments, an appropriate mixture of specific or control (irrelevant antigen) beads and a wash solution (phosphate-buffered saline and 1% bovine serum albumin supplied as part of the RhoCheck product) totaling 1.0 ml was centrifuged to concentrate the antigen beads. The supernatant was removed and replaced with fresh wash solution, and the centrifugation was repeated for three wash cycles to ensure that free antigen was not present in the solution. By altering the bead/wash solution mixture, various final bead concentrations were obtained. After the final centrifugation, an appropriate amount of supernatant was removed and antibody added so that the final antibody concentration in the mixture was 0.2 and 0.1 mg/ml [IgG and F(ab)]. Samples were incubated at 5°C for at least 12 h prior to experimentation.[7] Samples were drawn into 200-μm-thick glass capillary slides (W3520; Vitro Dynamics, Rockaway, NJ) for observation and experimentation conducted at 23 ± 2°C. Using this protocol, samples containing 18, 13.5, 9, and 4.5% by volume beads were obtained. In some experiments, the incubating antibody concentration was decreased to obtain larger immobile fractions. All samples were at a pH of 7.4.

Equipment for FRAP. The equipment, experimental procedure, and data analysis technique used in this study are those used by Kaufman and Jain (12). Briefly, the capillary slide was transilluminated for monitoring purposes at 480 nm by a mercury vapor lamp (Model HBO, 100 W; Zeiss, Morgan Instruments, Cincinnati, OH). Light passed through a heat reflector (Model Califax; Zeiss), heat absorber (Model KG-1; Zeiss), and fluorescein isothiocyanate exciter and red absorber filters (Models 46–79–79 and 46–78–85; Zeiss). The microscope was focused on the sample using a ×20 objective (Model F-LD 20/0.25, 46–06–05; Zeiss). Light emitted from the sample was passed through a barrier filter (Model 46–78–33; Zeiss) and the ×1.25 lens in a Zeiss Optovar (Model 47–16–45; Zeiss) installed in the microscope barrel. The image was monitored using an intensified charge coupled device (ICCD) camera (Model C2400–97; Hamamatsu, Photonic Microscopy, Inc., Oak Brook, IL) operated in a range where measured intensity was linear with fluorophore concentration. The video signal was sent to an image analysis system (DT-IRIS; Data Translation, Marlboro, MA) housed in an IBM PC-AT allowing on-line digital analysis of the image.

A 5-W argon ion laser (488 nm) (Model 2000–5; Spectra Physics, Mountain View, CA) was used to photobleach the sample. The laser beam was directed through a spatial filter (Model 900; Newport, Fountain Valley, CA) containing a ×10 objective (Model M-10X; Newport) and a 25-μm pinhole aperture (Model 900PH-25; Newport). The beam was then focused using a ×5 microscope objective (Model M-5X; Newport) and accessed the sample via the epiillumination port of the microscope where it was attenuated using neutral density filters (Models 46–78–40, -41, -42; Zeiss). Two shutters (Uniblitz Electronic; Vincent Associates, Rochester, NY) electronically controlled via the IBM PC-AT were used to control the bleaching time and light reaching the camera.

Experimental Procedure. Following prefluorescent and prebleach (background) image acquisition and storage, a region in the sample was photobleached for 0.08 to 0.18 s. Upon closing the laser shutter, the camera shutter was opened to allow imaging of the sample. Single video frames were acquired as rapidly as allowed by the acquisition board, requiring approximately 0.16 s for each frame. The fluorescence intensity data from the active region (bleach) were stored in the system buffers. To correct for nonuniform camera response or possible bleaching of the sample due to excitation light during fluorescence recovery, data were also obtained from a "control region." This control region was located distantly from the bleach. The process of data acquisition was continued for 24 s following the photobleach. After acquisition, background image subtraction, and correction for possible photobleaching due to the excitation light source, the intensity data from the first time point were low pass filtered. A minimum in fluorescence intensity was found to estimate the location of the bleached spot relative to the 90- x 70-pixel (69- x 69-μm) field of the active region. The bleach location was used to select a 36- x 29-pixel (28- x 28-μm) region properly centered about the photobleach (11, 12). The fluorescence intensity data in the 36- x 29-pixel region for the first time point as well as the average intensity in each 36- x 29-pixel region as a function of time were stored for subsequent analysis.

Data Analysis. Data analysis was performed on a Sun 3/260 workstation. A Gaussian profile was fit to the intensity data as a function of position from the first time point using the Levenberg-Marquardt (62, 63) nonlinear parameter estimation method. This fit determined bleach geometric parameters which were used to convert the data into dimensionless form and to calculate the dimensionless size of the active region, u (12). The diffusion coefficient and fraction of antibody which was immobile were obtained by using the Levenberg-Marquardt method to minimize the sum of squares error between the recovery equation given in Footnote 6 and the dimensionless average fluorescence intensity in the active region as a function of time. Many bleaches were performed upon each sample to obtain an average value of the diffusion coefficient and immobile fraction. Once corrected for the nonreactive fraction of antibody (12), nonlinear regression analysis was performed to obtain the equilibrium binding constant and concentration of binding sites from the immobile fraction *versus* antibody and bead concentration data (Equation F).

RESULTS

Results of Theoretical Assessment. Simulations of Lineweaver-Burk experiments did not demonstrate a dependence of the measured nonreactive fraction upon the cellular antigenic site density. An example of the Lineweaver-Burk analysis is

[6] The recovery equation (12) is

$$\frac{I_{Avg} - I_{TB}}{I_{TU} - I_{TB}} = 1 - \frac{\pi}{4u^2}\left\{(1-\phi_o)\mathrm{erf}^2\left(\frac{u}{\sqrt{1+8\frac{Dt}{R_o^2}}}\right) + \phi_o\mathrm{erf}^2 u\right\}$$

[7] Work by Nygren *et al.* (32, 54, 61) suggests that for some systems steady-state binding is not reached for this incubation time due to diffusion-limited binding and the extremely slow dissociation rate seen in solid-phase assays. To demonstrate that the immobile fractions of antibody measured here represent the equilibrium, steady-state value of antibody binding, a sample of 18% by volume VX2 antigen beads in 0.2 mg/ml of f-RVC-626 was incubated for 12 h, after which the diffusion coefficient and immobile fraction were measured. The sample was then reincubated for an additional 20 days, followed by a second photobleaching experiment. The diffusion coefficient and immobile fraction measured for the sample after 3 wk of incubation were not statistically different from those obtained following a 12-h incubation ($P = 0.37$ and 0.38 for D and ϕ, respectively). This demonstrates that the equilibrium level of binding was reached for this system after an overnight incubation.

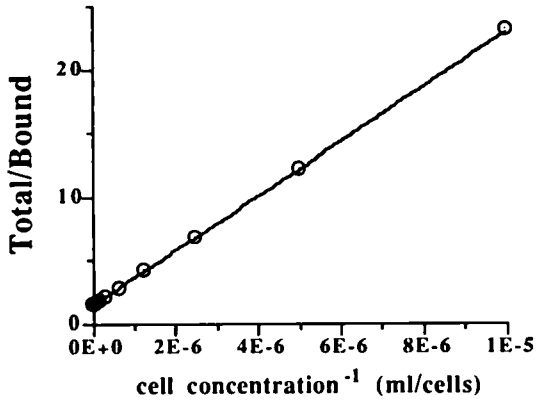

Fig. 3. Lineweaver-Burk plot to determine the nonreactive fraction of antibody. The total concentration of incubating antibody divided by the concentration of bound antibody is plotted *versus* the inverse of the incubating cellular concentration. In this simulation, the antigenic site density was 1×10^5 sites/cell. All other parameters are described in the text and given in Table 1. This analysis yielded the correct nonreactive fraction of 30%. *E* refers to the base 10 exponent of scientific notation.

shown in Fig. 3. Simulations conducted at site densities ranging between 5×10^3 and 5×10^6 sites/cell all yielded the nonreactive fraction input to the bivalent binding model. This result is to be expected since binding site excess was ensured through the selection of incubating antibody concentration. It should be noted that a different criterion in selecting antibody concentrations may have to be used for systems exhibiting a substantially lower intrinsic affinity.

Fig. 4 represents Scatchard, reciprocal, Langmuir, and FRAP plots, respectively, of the same cell binding experiment. Sips analysis for monovalent (Fig. 5*a*), and bivalent (Fig. 5*b*) binding is presented, where the antigenic site concentrations were taken from the Scatchard analysis. Note that, although all formulas are derived from Equation A and all are fit to the same data, there are differences in both their ability to demonstrate deviations from ideality and their best-fit kinetic parameters. This is due to the fact that the various algebraic transformations of Equation A cause the data points to be weighted differently with respect to optimizing the parameters. For instance, in Fig. 4*b*, the reciprocal plot condenses six of the data points to effectively act as one data point with respect to their ability to influence the shape of the fitted line. Deviation from the ideal homogeneous valence is not evidenced in the reciprocal, Langmuir, or FRAP plots but is evidenced in the slightly concave Scatchard plot in Fig. 4. These trends were apparent in all of the binding simulations, and it is clear that, of the above methods, the Scatchard analysis most clearly demonstrates deviations from ideality due to bivalent interaction. Boeynaems and Dumont (35) and DeLisi and Thakur (50) reached similar conclusions in their assessment of cooperativity and heterogeneous binding. Although the concave shape is readily apparent in Fig. 4*a*, in practice this trend may be obscured by experimental

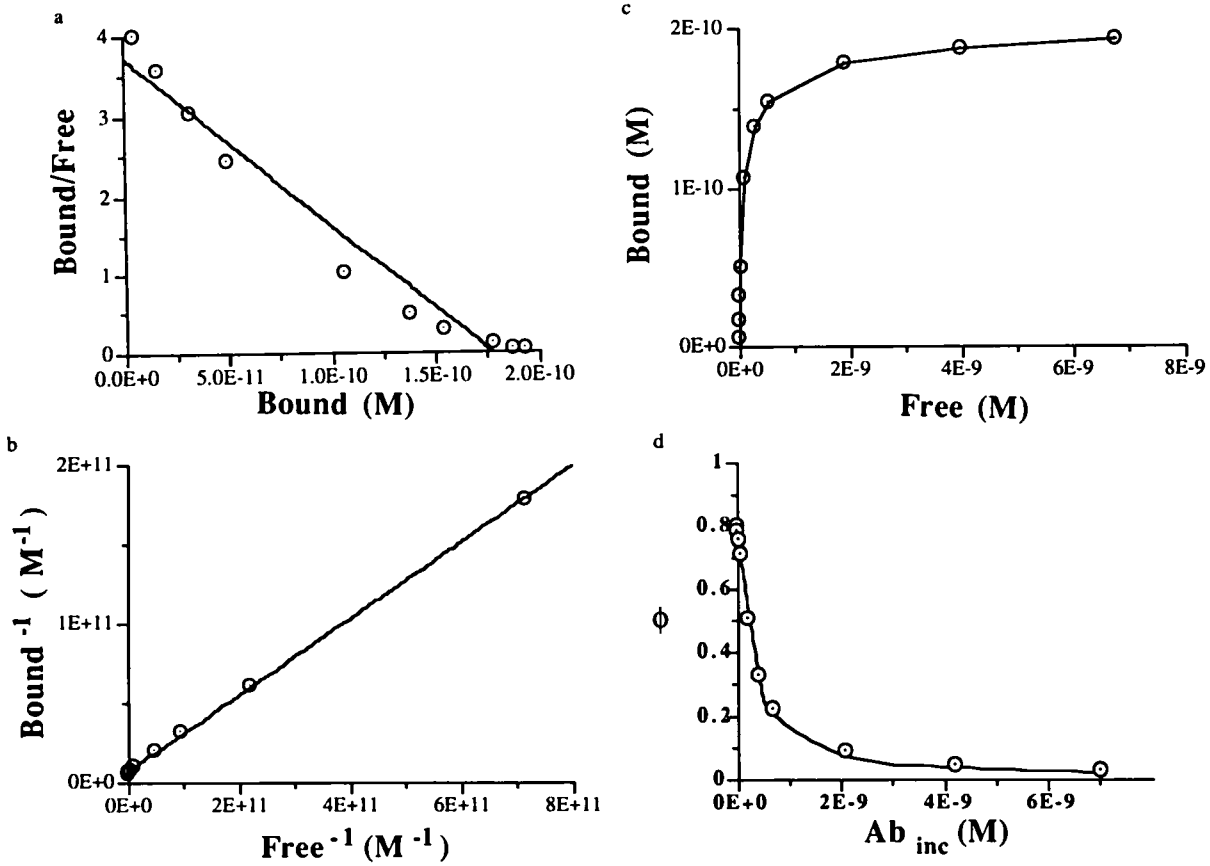

Fig. 4. Use of Scatchard (*a*), reciprocal (*b*), Langmuir (*c*), and FRAP (*d*) plots, respectively, to determine the antigenic concentration and equilibrium association constant. These simulations were conducted using a cellular antigenic site density of 2.5×10^5 sites/cell and an initial incubating antibody concentration of 1.0×10^{-11} M. All other parameters are as described in the text and given in Table 1. Despite the fact that all plots are derived from the same equation and use the same data set, the various plots yield slightly different parameter estimates and have varying capabilities in demonstrating deviations from ideality. In all cases the standard deviation of the estimated parameters was less than 10% of the parameter value. For this simulation, the estimated affinity binding constants were 2.1×10^{10}, 1.3×10^{10}, 2.7×10^{10}, and 2.5×10^{10} M^{-1}, and the antigenic site concentrations were 1.8×10^{-10}, 1.9×10^{-10}, 1.5×10^{-10}, and 1.5×10^{-10}M for the Scatchard, reciprocal, Langmuir, and FRAP analyses, respectively. The Scatchard plot best demonstrates the system's deviation from Equation A.

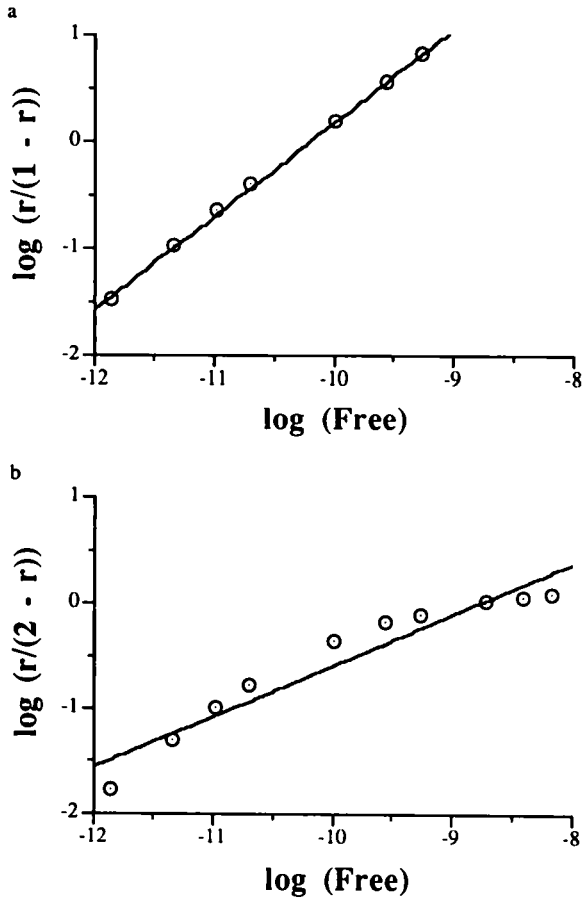

Fig. 5. Sips analysis when antigenic density is obtained from the Scatchard plot. This figure represents fits of the data used in Fig. 4 to Equations G and H representing monovalent and bivalent interaction, respectively. The antigenic site density used to calculate r values was obtained from the Scatchard analysis. The monovalent Sips analysis (a) fits the data well and yields an a value of 0.88 showing little deviation from ideality, whereas the bivalent Sips model (b) gives a deviation value of 0.49.

noise. Thus, deviation from the linear Scatchard form is not a reliable diagnostic of model nonconformity. The Sips analysis may prove more useful in this regard (see "Discussion").

Fig. 6 demonstrates the dependence of the Scatchard equilibrium binding constant upon both the antigenic site density of the cells and the initial incubating antibody concentrations used in a cell binding assay. It is seen that the estimated affinity may range over four orders of magnitude for a similar range in cellular antigenic site density. In addition, the choice of initial incubating antibody concentration may alter the measured affinity by a factor of two. The equilibrium binding constant obtained through Scatchard analysis did not vary when the cellular concentration is varied over four decades at constant cellular antigen density. While deviation from Equation C is graphically evident in some of the simulations performed, this deviation may often be obscured in practice by experimental noise or sparse data. Even when such deviation is observable, it is often ignored (39, 64).

When binding assays are conducted using purified antigen immobilized to the bottom of cell culture wells, the bulk concentration of any component X will be equal to $X_s\gamma$. γ is defined as the ratio of plate area to incubating antibody volume.[8] If cell assays and plate assays are conducted with equal bulk concentrations of antigen, $[Ag]_s$ for the cell assay will be larger than $[Ag]_s$ for the plate assay by a factor of

$$\frac{\gamma}{4\pi r_c^2\left(\frac{\text{no. of cells}}{\text{cm}^3}\right)}.$$

As predicted by Equation X, for experiments conducted with identical incubating antibody concentrations in systems where bivalent binding predominates, the observed equilibrium constant using a cell assay will be larger than that in a plate assay by this same factor. This demonstrates that the form of immobilized antigen is yet another source of parameter variation when equilibrium binding experiments are conducted with multivalent systems. These trends of increased avidity with decreased system dimensionality have been evidenced experimentally in comparisons of homogeneous and heterogeneous binding assays (32, 61).

Results of Photobleaching Experiments. The diffusion coefficients and immobile fractions obtained through photobleaching for the F(ab) and IgG antibodies are shown in Tables 2 and 3, respectively. Also shown are the nonreactive fractions measured using fluorometry (12). The measured diffusion coefficients were independent of sample preparation (one-way analysis of variance $P = 0.73$ and 0.88 for the F(ab) and IgG, respectively). Slight immobilization was noted in the irrelevant antigen sample. This immobilization was subtracted when converting from the immobile fraction of fluorescent material to the fraction of biologically active material as in Ref. 12. Fig.7 shows the fit of the F(ab) data to Equation F to obtain the kinetic parameters given in Table 2. An antigen dilution factor of 1 corresponded to an 18% by volume solution of antigen beads. Thus, the concentration of binding sites reported is for this volume fraction. An antibody dilution factor of 1 corresponded to a total antibody concentration of 2.07×10^{-6} M for the F(ab) antibody.

Use of Bivalent Model to Predict FRAP Results. The validity and utility of the bivalent model were assessed through its ability to predict photobleaching results for the IgG antibody, based upon kinetic parameters obtained in F(ab) experiments. Equations S to V were used to generate plots of predicted immobile fractions *versus* antibody and antigen dilution factors for the bivalent interaction of IgG RVC-626 with the VX2 antigen

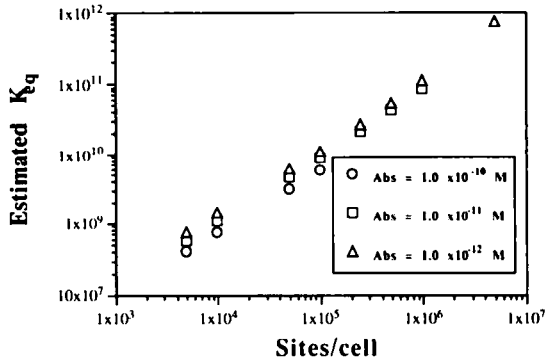

Fig. 6. Estimated equilibrium binding constant (K_{eq}) as a function of antigenic site density and initial incubating antibody concentration. Scatchard simulations were conducted as described in the text. The resulting affinity is seen to depend quite heavily upon the binding site density and is also dependent upon the experimental protocol. It is clear that experiments conducted upon identical antibody/antigen pairs, having an identical intrinsic affinity, may yield reported affinities divergent by orders of magnitude.

[8] The value of γ used in these simulations is given in Table 1. It is calculated assuming that 20 μl of antibody are added to a culture well 0.6 cm in diameter and that all antigen exists at the well bottom.

Table 2 *Results of photobleaching experiments for F(ab) RVC-626*

Values are reported as the mean ± SD. Sample identification is as follows: 1, 2.1×10^{-6} M F(ab) in 18% by volume control beads; 2, 2.1×10^{-6} M F(ab) in 4.5% by volume antigen beads; 3, 2.1×10^{-6} M F(ab) in 9% by volume antigen beads; 4, 2.1×10^{-6} M F(ab) in 13.5% by volume antigen beads; 5, 2.1×10^{-6} M F(ab) in 18% by volume antigen beads; 6, 1.1×10^{-6} M F(ab) in 18% by volume antigen beads.

Sample	D ($\times 10^7$ cm²/s)	ϕ_0	n
1	6.99 ± 0.57	0.05 ± 0.02	18
2	6.65 ± 0.53	0.09 ± 0.02	9
3	6.80 ± 0.62	0.13 ± 0.01	16
4	6.77 ± 0.79	0.15 ± 0.03	23
5	7.12 ± 0.58	0.16 ± 0.02	10
6	6.82 ± 0.45	0.16 ± 0.02	8
	$nr = 0.83$		
		$K = 2.9 \pm 1.1 \times 10^6$ M^{-1}	
		$Ag_o = 8.3 \pm 2.3 \times 10^{-7}$ M	

Table 3 *Results of photobleaching experiments for IgG RVC-626*

Values are reported as the mean ± SD. Sample identification is as follows: 1, 1.3×10^{-6} M IgG in 18% by volume control beads; 2, 1.3×10^{-6} M IgG in 4.5% by volume antigen beads; 3, 1.3×10^{-6} M IgG in 9% by volume antigen beads; 4, 1.3×10^{-6} M IgG in 13.5% by volume antigen beads; 5, 1.3×10^{-6} M IgG in 18% by volume antigen beads; 6, 2.6×10^{-6} M IgG in 18% by volume antigen beads; 7, 6.5×10^{-7} M IgG in 18% by volume antigen beads.

Sample	D ($\times 10^7$ cm²/s)	ϕ_0	n
1	4.54 ± 0.65	0.03 ± 0.03	11
2	4.59 ± 1.06	0.11 ± 0.05	13
3	4.80 ± 0.87	0.19 ± 0.05	16
4	4.67 ± 1.52	0.30 ± 0.10	10
5	4.81 ± 1.00	0.31 ± 0.06	29
6	4.40 ± 0.41	0.25 ± 0.06	8
7	4.97 ± 1.42	0.34 ± 0.07	17
	nr = 0.67		

beads. The values of K_1 and Ag_o were taken from the photobleaching experiments of the monovalent F(ab) RVC-626, after dividing K by 2 to be consistent with the nomenclature of Equations A and I. The antigen bead size was determined using a Coulter Counter ZM (Coulter Electronics, Limited, Luton, England) and Coulter Channelyzer 256 (Coulter Electronics, Limited). Using these instruments, the diameter of the antigen beads was found to be 1.60 ± 0.40 μm. With this parameter and the volume percentage of beads in solution, the bead concentration was obtained. ϕ was then calculated assuming $\langle r \rangle$ equal to 87 Å. With these values fixed, there were no adjustable parameters in the model. The curves in Fig. 8 represent the bivalent binding model's prediction of the IgG FRAP experiments. With the exception of data with large antibody concentrations, quantitative agreement between the theoretical model and the actual data is quite good. The average relative error for the prediction of IgG data (with no adjustable parameters) was 0.06%. This may be compared to the fit of the F(ab) data (with two adjustable parameters) of 0.04%.

DISCUSSION

It has been demonstrated that the estimated affinity of a monoclonal antibody may vary over four orders of magnitude, depending upon both the experimental protocol and conditions. This may explain both the apparent discrepancy between monoclonal antibodies' reported affinity and their *in vivo* distribution, and the differences in affinities reported for identical antibody/antigen pairs. In addition, it raises questions about the utility of equilibrium binding experiments using potentially multivalent ligand where the conditions affecting ligand valence are varied. Since the avidity of a bivalent antibody for its specific antigen will always be a function of the experimental conditions, the intrinsic affinity of the monovalent interaction is the fundamental parameter of interest in equilibrium binding experiments. With knowledge of the intrinsic affinity, the avidity of the interaction in an experimental system of interest may be predicted using the proposed model of bivalent interaction as done in this study. Resolution of equilibrium binding data using bivalent antibody does not provide an adequate method for determining the intrinsic affinity. Equilibrium binding experiments performed using bivalent antibody should be repeated using the monovalent form of the antibody in order to provide this parameter.

Varying measurements of affinities for identical antibody/antigen pairs are common in the literature. While there are several biological mechanisms that may account for these differences (24, 35, 52–54), many of the discrepancies may be explained by the above model of bivalent interaction. One particular example is the investigation of the affinity of bivalent B72.3 monoclonal antibody for the tumor-associated antigen TAG-72. It should not be surprising that Muraro *et al.* (16), using a plate assay with a large concentration of highly purified TAG-72, reported an affinity 100 times greater than that obtained by Kaufman and Jain (12), whose immobilized antigen consisted of tumor cell homogenate immobilized onto microscopic beads. If the influence of bivalent interaction cannot be discerned and properly accounted for in equilibrium binding experiments, kinetic parameters obtained through these methods should be used with caution.

Of the numerous variations of Equation A used for the purposes of kinetic parameter estimation, the Scatchard plot seems best suited to graphically depict system deviation from the model of homogeneous, one-step, reversible binding. In practice, however, experimental noise or paucity of data may obscure this deviation. Sips plots, as a validation of system conformity, must be used with care. As seen in Fig. 5*a*, when the data are normalized using parameters obtained via Scatchard analysis, the monovalent Sips plot does not suggest deviation from Equation A. This is due to the fact that deviation from this equation is already incorporated into $[Ag_o]$ through the error of the Scatchard fit. By this same argument, when the bivalent

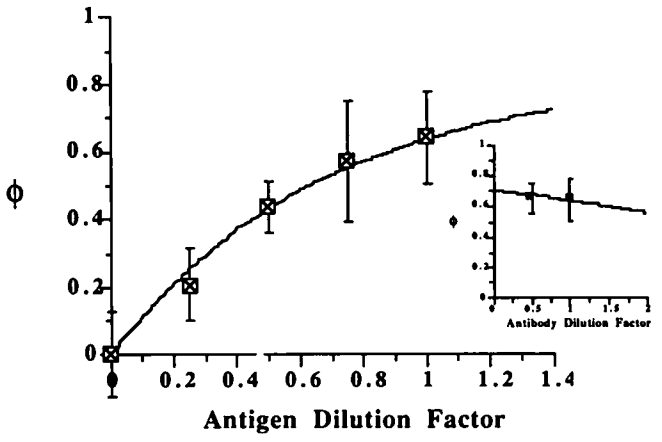

Fig. 7. Fit to obtain K and Ag_o for F(ab) RVC-626. Nonreactive antibody-corrected immobile fractions (ϕ_c) as a function of antigen dilution at a constant incubating antibody concentration and as a function of incubating antibody concentration at a constant antigen concentration were fit to Equation F to obtain the equilibrium binding constant and antigen concentration for a 18% by volume solution of antigen beads. *Bars* represent the standard deviation of the measurement. *Antigen Dilution Factor* refers to the relative decrease in antigen concentration with respect to 18% by volume antigen beads. Similarly, *Antibody Dilution Factor* refers to the relative decrease in antibody concentration with respect to 2.07×10^{-6} M F(ab) (*inset*).

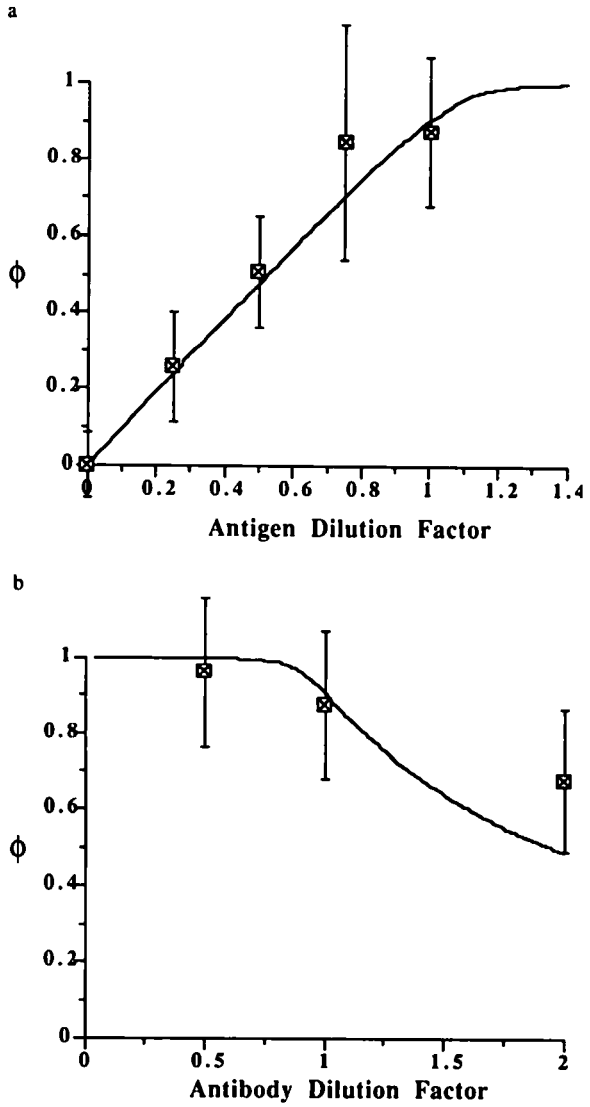

Fig. 8. Verification of bivalent model through its ability to predict IgG RVC-626 binding data. Nonreactive antibody-corrected immobile fractions (ϕ_c) as a function of antigen dilution at a constant incubating antibody concentration (*a*) and as a function of incubating antibody concentration at a constant antigen concentration (*b*) were plotted as in Fig. 7. *Bars* represent the standard deviation of the measurement. *Antigen Dilution Factor* (*a*) refers to the relative decrease in antigen concentration with respect to 18% by volume antigen beads. Similarly, *Antibody Dilution Factor* (*b*) refers to the relative decrease in antibody concentration with respect to 1.33×10^{-6} M IgG. Using the bivalent binding model of Crothers and Metzger (22) and the intrinsic kinetic parameters found through photobleaching the F(ab), these data were predicted *a priori* with no adjustable parameters (*a* and *b curves*). The quantitative agreement between the model and the data is quite good with the exception of high antibody concentrations.

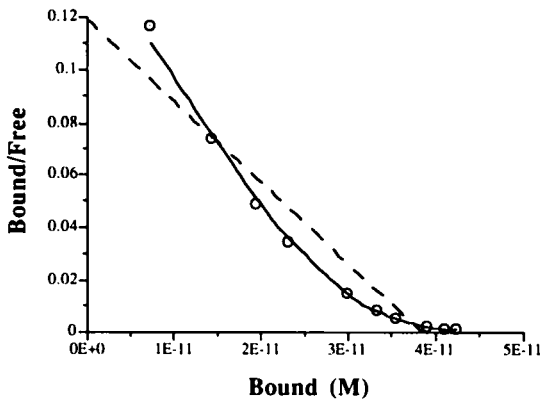

Fig. 9. Approach to resolve bivalent Scatchard plot into monovalent and bivalent components. This Scatchard plot was generated using an antigen density of 5.0×10^4 sites/cell, an initial incubating antibody concentration of 1×10^{-10} M, and the baseline parameters given in Table 1 and in the text. This yielded a bulk concentration of antigen of 8.3×10^{-11}M. One % of the bound antibody is monovalently bound at an incubating antibody concentration of 1.0×10^{-10}M, whereas 15% is monovalently bound at 1×10^{-7}M. When the data are fit to Equation C (*dashed line*), the resulting parameters are $K = 3.1 \times 10^9 M^{-1}$ and $Ag_o = 3.8 \times 10^{-11}$M. The resolved plot suggested in Ref. 48 for the purposes of antibody heterogeneity (*solid line*) fits the data well but yields $K_1 = 8.2 \times 10^7 M^{-1}$, $Ag_{o1} = 1.4 \times 10^{-11}$M, $K_2 = 4.6 \times 10^9 M^{-1}$, and $Ag_{o2} = 3.1 \times 10^{-11}$M with standard deviations on each of the parameter estimates less than 10% of the parameter value. The method of Roholt *et al.* fails to correctly report the intrinsic affinity even though the simulation is conducted in antibody excess. Resolution of this type cannot be universally used to obtain an accurate estimate of the intrinsic affinity. A larger range or greater concentration of incubating antibody does not improve the resolution.

Sips equation (Equation H) is fit to the same data, it is guaranteed to yield a low value of the deviation constant, since the parameter used to normalize the data assumes monovalent interaction. Sips plots should more properly use a value of $[Ag_o]$ obtained through monovalent equilibrium binding experiments when normalizing the data. When this was performed, the two Sips plots yielded values of 0.47 and 0.42 for the monovalent and bivalent models, respectively.

Since the upward slope of the Scatchard plot due to bivalent interaction is of a similar shape as the deviation produced by negative cooperativity, binding site or antibody heterogeneity, and endocytosis of the bound complex, it may be argued that techniques developed to dissect these complexities may also be applied to that of a bivalent monoclonal antibody. In particular, it might seem as though the methods developed for the resolution of an upwardly sloping Scatchard curve due to binding site heterogeneity into the summation of linear portions (one for each type of site) (45–51) may be applied in order to determine the intrinsic affinity and percentage bound monovalently, as well as the bivalent avidity and the percentage of bivalently bound antibody. For Scatchard plots with pronounced curvature, the data may be fit to the heterogeneous binding model suggested by Roholt *et al.* (Footnote 9; Ref. 48; Fig. 9). However, this procedure fails to accurately yield the intrinsic affinity. In addition, the curvature must be quite pronounced in order to provide statistically independent parameters in this model. The use of more data points or larger incubating antibody concentrations also fails in this regard due to the fact that the avidity and proportion of monovalent to bivalent sites are not constant with respect to incubating antibody concentration. This is fundamentally different from the situation of heterogeneous binding sites, where the population statistics and affinities are constant for all incubating antibody concentrations.

It is also tempting to use numerical solution of Equations S to V to fit bivalent equilibrium data to the three intrinsic parameters K_1, Ag_o, and ϕ. This should be accompanied by proper statistical analysis (65) to ensure that all parameters are statistically independent. Such a fit of the data displayed in Fig. 8 would serve as an additional confirmation of the theoretical model, but the parameters could not be determined independently from the current data set.

[9] Roholt *et al.* (48) derive that for an antibody binding to two different antigenic sites with differing affinities, the ratio of bound to free antibody will be

$$\frac{[B]}{[Ab]} = [Ag_{o1}]K_1(1 + [Ab]K_2) + [Ag_{o2}]K_2(1 + [Ab]K_1) - [B](K_1 + K_2 + [Ab]K_1K_2)$$

Ultimately, the intrinsic affinity must be measured directly, in separate experiments as performed here. This intrinsic affinity and the concentration of binding sites for monovalent attachment are true constants that may be utilized for comparing and ranking the strength of the antibody/antigen interaction, unlike parameters obtained in equilibrium binding experiments of bivalent antibody which are not unique. The use of monovalent fragments may also reduce complications due to receptor endocytosis and clustering seen in bivalent studies. It has been demonstrated that the strength of bivalent interaction may be accurately predicted with knowledge of the monovalent kinetic parameters using the model of Crothers and Metzger (22) with no adjustable parameters. As discussed previously, this model fails at high extents of saturation due to the use of average binding site concentrations rather than a statistical mechanical model of the bead surface. Nevertheless, the proposed model of avidity enhancement may be used as a predictive tool in a variety of experimental and clinical protocols. The model also demonstrates quite convincingly the ambiguity of bivalent equilibrium binding experiments. With an appreciation for the enhanced avidity afforded by bivalent binding, it is hoped that more meaningful correlations between affinity and *in vivo* distribution may be resolved, and that ultimately, more effective antibody therapies may be designed.

ACKNOWLEDGMENTS

The authors thank D. Mackensen and B. Rhodes for providing the reagents necessary for this work and for their valuable collaboration and suggestions. They also thank Dr. E. Ko, Dr. F. Yuan, and Dr. L. Baxter for their suggestions and Dr. M. Domach for the use of equipment in his laboratory.

REFERENCES

1. Jain, R. K. Delivery of novel therapeutic agents in tumors: physiological barriers and strategies. J. Natl. Canc. Inst., *81:* 570–576, 1989.
2. Weinstein, J. N., Parker, R. J., Keenan, A. M., Dower, S. K., Morse, H. C., and Sieber, S. M. Monoclonal antibodies in the lymphatics: towards the diagnosis and therapy of tumor metastases. Science (Washington DC), *218:* 1334–1337, 1982.
3. Dedrick, R. L., and Flessner, M. F. Pharmacokinetic considerations on monoclonal antibodies. *In:* M. S. Mitchell (ed.), Immunity to Cancer, Vol. II, pp. 429–438, New York: Alan R. Liss, 1989.
4. Fujimori, K., Covell, D. G., Fletcher, J. E., and Weinstein, J. N. Modeling analysis of the global and microscopic distribution of immunoglobulin G, $F(ab')_2$, and Fab in tumors. Cancer Res., *49:* 5656–5663, 1989.
5. Thomas, G. D., Chappell, M. J., Dykes, P. W., Ramsden, D. B., Godfrey, K. R., Ellis, J. R. M., and Bradwell, A. R. Effect of dose, molecular size, affinity, and protein binding on tumor uptake of antibody or ligand: a biomathematical model. Cancer Res., *49:* 3290–3296, 1989.
6. Baxter, L. T., and Jain, R. K. Transport of fluid and macromolecules in tumors. III. Role of binding and metabolism. Microvasc. Res., *41:* 5–23, 1991.
7. Baxter, L. T., and Jain, R. K. Transport of fluid and macromolecules in tumors. IV. A microscopic model of perivascular distribution. Microvasc. Res., *41:* 252–272, 1991.
8. Shockley, T. R., Lin, K., Sung, C., Nagy, J. A., Tompkins, R. G., Dedrick, R. L., Dvorak, H. F., and Yarmush, M. L. A quantitative analysis of tumor-specific monoclonal antibody uptake in human melanoma xenografts: effects of antibody immunological properties and tumor antigen expression levels. Cancer Res., *52:* 357–366, 1992.
9. Sung, C., Shockley, T. R., Morrison, P. M., Dvorak, H. F., Yarmush, M. L., and Dedrick, R. L. Predicted and observed effects of antibody affinity and antigen density on monoclonal antibody uptake in solid tumors. Cancer Res., *52:* 377–384, 1992.
10. Schlom, J., Eggensperger, D., Colcher, D., Molinolo, A., Houchens, D., Miller, L. S., Hinkle, G., and Siler, K. Therapeutic advantage of high-affinity anticarcinoma radioimmunoconjugates. Cancer Res., *52:* 1067–1072, 1992.
11. Kaufman, E. N., and Jain, R. K. Quantification of mass transport and binding parameters using fluorescence recovery after photobleaching: potential for *in vivo* applications. Biophys. J., *58:* 873–885, 1990.
12. Kaufman, E. N., and Jain, R. K. Measurement of mass transport and reaction parameters in bulk solution using photobleaching: the reaction limited binding regime. Biophys. J., *60:* 596–610, 1991.
13. Steward, M. W., and Steensgaard, J. Antibody Affinity: Thermodynamic Aspects and Biological Significance. Boca Raton, FL: CRC Press, 1983.
14. McCready, D. R., Balch, C. M., Fidler, I. J., and Murray, J. L. Lack of comparability between binding of monoclonal antibodies to melanoma cells *in Vitro* and localization *in Vivo*. J. Natl. Cancer Inst., *81:* 682–687, 1989.
15. Sharkey, R. M., Gold, D. V., Aninpot, R., Vagg, R., Ballance, C., Newman, E. S., Ostella, F., Hansen, H. J., and Goldenberg, D. M. Comparison of tumor targetting in nude mice by murine monoclonal antibodies directed against different human colorectal cancer antigens. Cancer Res., *50* (Suppl.): 828s–834s, 1990.
16. Muraro, R., Kuroki, M., Wunderlich, D., Poole, D. J., Colcher, D., Thor, A., Greiner, J. W., Simpson, J. F., Molinolo, A., Noguchi, P., and Schlom, J. Generation and characterization of B72.3 second generation monoclonal antibodies reactive with tumor-associated glycoprotein 72 antigen. Cancer Res., *48:* 4588–4596, 1988.
17. Milenic, D. E., Yokota, T., Filpula, D. R., Finkelman, M. A. J., Dodd, S. W., Wood, J. F., Whitlow, M., Snoy, P., and Schlom, J. Construction, binding properties, metabolism, and tumor targeting of a single chain Fv derived from the pancarcinoma monoclonal antibody CC49. Cancer Res., *51:* 6363–6371, 1991.
18. Neumaier, M., Shively, L., Chen, F. S., Gaida, F. J., Ilgen, C., Paxton, R. J., Shively, J. E., and Riggs, A. D. Cloning of the genes for T84.66, an antibody that has a high specificity and affinity for carcinoembryonic antigen, and expression of chimeric human/mouse T84.66 Genes in myeloma and Chinese hamster ovary cells. Cancer Res., *50:* 2128–2134, 1990.
19. Beatty, B. G., Beatty, J. D., Williams, L. E., Paxton, R. J., Shively, J. E., and O'Conner-Tressel, M. Effect of specific antibody pretreatment on liver uptake of ^{111}In-labeled anticarcinoembryonic antigen monoclonal antibody in nude mice bearing human colon cancer xenografts. Cancer Res., *49:* 1587–1594, 1989.
20. Friedman, E., Thor, A., Hand, P. H., and Schlom, J. Surface expression of tumor-associated antigens in primary cultured human colonic epithelial cells from carcinomas, benign tumors, and normal tissues. Cancer Res., *45:* 5648–5655, 1985.
21. Hand, P. H., Colcher, D., Salomon, D., Ridge, J., Noguchi, P., and Schlom, J. Influence of spatial configuration of carcinoma cell populations on the expression of a tumor-associated glycoprotein. Cancer Res., *45:* 833–840, 1985.
22. Crothers, D. M., and Metzger, H. The influence of polyvalency on the binding properties of antibodies. Immunochemistry, *9:* 341–357, 1972.
23. DeLisi, C. Antigen Antibody Interactions. Berlin: Springer-Verlag, 1976.
24. DeLisi, C., and Chabay, R. The influence of cell surface receptor clustering on the thermodynamics of ligand binding and the kinetics of dissociation. Cell Biophys., *1:* 117–131, 1979.
25. Reynolds, J. A. Interaction of divalent antibody with cell surface antigens. Biochemistry, *18:* 264–269, 1979.
26. Perelson, A. S., Goldstein, B., and Rocklin, S. Optimal strategies in immunology. III. The IgM-IgG switch. J. Math. Biol., *10:* 209–256, 1980.
27. Dower, S. K., DeLisi, C., Titus, J. A., and Segal, D. M. Mechanism of binding of multivalent immune complexes to Fc receptors. 1. Equilibrium binding. Biochemistry, *20:* 6326–6334, 1981.
28. Waite, B. A., and Chang, E. L. Antibody multivalency effects in the direct binding model for vesicle immunolysis assays. J. Immunol. Methods, *115:* 227–238, 1988.
29. Pisarchick, M. L., and Thompson, N. L. Binding of a monoclonal antibody and its Fab fragment to supported phospholipid monolayers measured by total internal reflection microscopy. Biophys. J., *58:* 1235–1249, 1990.
30. Hornick, C. L., and Karush, F. Antibody affinity. III. The role of multivalence. Immunochemistry, *9:* 325–340, 1972.
31. Dower, S. K., Ozato, K., and Segal, D. M. The interaction of monoclonal antibodies with MHC Class I antigens on mouse spleen cells. I. Analysis of the mechanism of binding. J. Immunol., *132:* 751–758, 1984.
32. Nygren, H., Czerkinsky, C., and Stenberg, M. Dissociation of antibodies bound to surface-immobilized antigen. J. Immunol. Methods, *85:* 87–95, 1985.
33. Holton, O. D., Black, C. D., Parker, R. J., Covell, D. G., Barbet, J., Sieber, S. M., Talley, M. J., and Weinstein, J. N. Biodistribution of monoclonal IgG1, $F(ab')_2$, and Fab' in mice after intravenous injection: comparison between antiB cell (anti-LyB8.2) and irrelevant (MOPC-21) antibodies. J. Immunol., *139:* 3041–3049, 1987.
34. Le Doussal, J. M., Gruaz-Guyon, A., Martin, M., Gautherot, E., Delaage, M., and Barbet, J. Targeting of indium 111-labeled bivalent hapten to human melanoma mediated by bispecific monoclonal antibody conjugates: imaging of tumors hosted in nude mice. Cancer Res., *50:* 3445–3452, 1990.
35. Boeynaems, J. M., and Dumont, J. E. Quantitative analysis of the binding of ligands to their receptors. J. Cyclic Nucleotide Res., *1:* 123–142, 1975.
36. Builder, S. E., and Segel, I. H. Equilibrium ligand binding assays using labeled substrates: nature of the errors introduced by radiochemical impurities. Anal. Biochem., *85:* 413–424, 1978.
37. Reimann, E. M., and Soloff, M. S. The effect of radioactive contaminants on the estimation of binding parameters by Scatchard analysis. Biochim. Biophys. Acta, *533:* 130–139, 1978.
38. Lineweaver, H., and Burk, D. The determination of enzyme dissociation constants. J. Am. Chem. Soc., *56:* 658–666, 1934.
39. Badger, C. C., Krohn, K. A., and Bernstein, I. D. *In vitro* measurement of avidity of radioiodinated antibodies. Nucl. Med. Biol., *14:* 605–610, 1987.

40. Scatchard, G. The attractions of proteins for small molecules and ions. Ann. NY Acad. Sci., *51:* 660–672, 1949.
41. Steward, M. W., and Petty, R. E. The antigen-binding characteristics of antibody pools of different relative affinity. Immunology, *23:* 881–887, 1972.
42. Langmuir, I. The constitution and fundamental properties of solids and liquids. Part I. Solids. J. Am. Chem. Soc., *38:* 2221–2295, 1916.
43. Sips, R. On the structure of a catalyst surface. J. Chem. Phys., *16:* 490–496, 1948.
44. Hill, A. V. A new mathematical treatment of changes in ionic concentration in muscle and nerve under the action of electric currents, with a theory as to their mode of excitation. J. Physiol., *40:* 190–224, 1910.
45. Hart, H. E. Determination of equilibrium constants and maximum binding capacities in complex *In Vitro* systems. I. The mammillary system. Bull. Math. Biophys., *27:* 216–225, 1965.
46. Rosenthal, H. E. A graphic method for the determination and presentation of binding parameters in a complex system. Anal. Biochem., *20:* 525–532, 1967.
47. Klotz, I. M., and Hunston, D. L. Properties of graphical representations of multiple classes of binding sites. Biochemistry, *10:* 3065–3069, 1971.
48. Roholt, O. A., Grossberg, A. L., Yagi, Y., and Pressman, D. Limited heterogeneity of antibodies. Resolution of hapten binding curves into linear components. Immunochemistry, *9:* 961–965, 1972.
49. Rubinow, S. I. A suggested method for the resolution of Scatchard plots. Immunochemistry, *14:* 573–576, 1977.
50. DeLisi, C., and Thakur, A. K. An analysis of the limits of resolution of binding experiments as assays for affinity heterogeneity. Immunochemistry, *15:* 389–391, 1978.
51. Nôrby, J. G., Ottolenghi, P., and Jensen, J. Scatchard Plot: common misinterpretation of binding experiments. Anal. Biochem., *102:* 318–320, 1980.
52. Gex-Fabry, M., and DeLisi, C. Receptor-mediated endocytosis: a model and its implications for experimental analysis. Am. J. Physiol., *247:* R768–R779, 1984.
53. DeLisi, C., and Metzger, H. Some physical chemical aspects of receptor-ligand interactions. Immunol. Commun., *5:* 417–436, 1976.
54. Nygren, H., Werthen, M., and Stenberg, M. Kinetics of antibody binding to solid-phase-immobilized antigen: effect of diffusion rate limitation and steric interaction. J. Immunol. Methods, *101:* 63–71, 1987.
55. Stenberg, M., and Nygren, H. Kinetics of antigen-antibody reactions at solid-liquid interfaces. J. Immunol. Methods, *113:* 3–15, 1988.
56. DeLisi, C., and Crothers, D. M. The contribution of proximity and orientation to catalytic reaction rates. Biopolymers, *12:* 1689–1704, 1973.
57. Steller, M. A., Parker, R. J., Covell, D. G., Holton, O. D., Keenan, A. M., Seiber, S. M., and Weinstein, J. N. Optimization of monoclonal antibody delivery via the lymphatics: the dose dependence. Cancer Res., *46:* 1830–1834, 1986.
58. Wilson, B. S., Petrella, E., Lowe, S., Lien, K., Mackensen, D. G., Gridley, D. S., and Stickney, D. R. Radiolocalization of small cell lung cancer and antigen-positive normal tissues using monoclonal antibody LS2D617. Cancer Res., *50:* 3124–3130, 1990.
59. Lindmo, T., Boven, E., Cuttitta, F., Fedorko, J., and Bunn, P. A. Determination of the immunoreactive fraction of radiolabeled monoclonal antibodies by linear extrapolation to binding at infinite antigen excess. J. Immunol. Methods, *72:* 77–89, 1984.
60. Kidd, J. G., and Rous, P. A. A transplantable rabbit carcinoma originating in a virus-induced papilloma and containing the virus in a masked or altered form. J. Exp. Med., *71:* 132–138, 1940.
61. Nygren, H., Kaartinen, M., and Stenberg, M. Determination by ellipsometry of the affinity of monoclonal antibodies. J. Immunol. Methods, *92:* 219–225, 1986.
62. Levenberg, K. A method for the solution of certain problems in least squares. Q. Appl. Math., *2:* 164–168, 1944.
63. Marquardt, D. An algorithm for least squares estimation of nonlinear parameters. SIAM J. Appl. Math., *11:* 431–441, 1963.
64. Kalofonos, H., Rowlinson, G., and Epenetos, A. A. Enhancement of monoclonal antibody uptake in human colon xenografts following irradiation. Cancer Res., *50:* 159–163, 1990.
65. Caracotsios, M. Model parametric sensitivity analysis and nonlinear parameter estimation. Theory and applications (thesis). Ph.D. Thesis, Department of Chemical Engineering, University of Wisconsin, Madison, 1986.